Applied Surface Science 563 (2021) 150285

Contents lists available at ScienceDirect

Applied Surface Science

journal homepage: www.elsevier.com/locate/apsusc

Full Length Article

# Deposition and characterisation of sputtered molybdenum oxide thin films with hydrogen atmosphere

Nicolau Lopez-Pinto [a,b], Thomas Tom [a,b], Joan Bertomeu [a,b,*], Jose Miguel Asensi [a,b], Eloi Ros [c], Pablo Ortega [c], Cristobal Voz [c]

[a] Departament de Física Aplicada, Universitat de Barcelona, Barcelona, Spain
[b] Institute of Nanoscience and Nanotechnology (IN2UB), Universitat de Barcelona, Barcelona, Spain
[c] Universitat Politècnica de Catalunya, Barcelona, Spain

ARTICLE INFO

*Keywords:*
$MoO_3$ thin films
Reactive sputtering
Hydrogen atmosphere
Reduced molybdenum oxide

ABSTRACT

Sputtered films of reduced molybdenum oxide ($MoO_x$) with a molybdenum trioxide target in different pressures and atmospheres were deposited in varying temperatures. Compositional, optic, and electric characteristics of the samples were studied. X-ray photoelectron spectroscopy revealed reduced states when working in the hydrogen + argon atmosphere implying that stoichiometry could be controlled by adding some hydrogen in the sputtering chamber. The effect of slightly increasing the substrate temperature during deposition was also studied and lead to the presence of metastable $Mo^{4+}$ states at 3 mTorr. Optical properties match the ones already in the literature, and transmittances of 90% were achieved. The results support sputtering as a viable method of depositing $MoO_x$ films apart from thermal evaporation for many applications.

## 1. Introduction

During the last decades, transition metal oxides (TMOs) have been a matter of interest for their many applications [1,2]. In this paper, the focus is specifically on molybdenum oxide due to its use as a hole collector and anti-reflective coating in solar cells [3–7], hole injection or buffer layer in OLEDs [8,9], micro batteries [10] and gas sensors [11–13], as well as many others. Molybdenum oxide exhibits advantageous structural, chemical and optical properties [14–16].

This study aims to find a suitable replacement for the doped amorphous silicon layer that acts as a hole transport layer (HTL) in the solar cells as proposed in [3,4], by adopting a more industrial method of sputtering for molybdenum trioxide ($MoO_3$). This deposition method may have an interest in the industry sector, as not only it is easier to implement than evaporation, but also a simpler fabrication process than the ones being used nowadays.

There are several studies of molybdenum oxide deposited by sputtering in reactive atmospheres for different applications, many of them involving a metallic target with an $O_2$ reactive atmosphere [13,17–25] or involving other materials [26–28] but none of them includes purely molybdenum oxide incorporating $H_2$ in the atmosphere. In this study different thin film samples of molybdenum oxide have been deposited in different atmospheres (Ar, Ar:$O_2$, and Ar:$H_2$) by sputtering from a ceramic $MoO_3$ target, and the results on their compositional, optical and electric analysis are to be reported. The Ar:$H_2$ atmosphere should let us control the final composition because the hydrogen is expected to intercalate into the oxide, forming hydrogen molybdenum bronzes [29]. Those will cause small crystallographic rearrangements. Association of hydrogen with oxygen to form water molecules that will eventually leave the film should occur, and the molybdenum oxide should reduce, acquiring a bluish color [30,31].

In the case of samples prepared in the Ar:$H_2$ atmosphere, deposition temperature has been increased to create more oxygen vacancies, similarly to what occurs when depositing indium tin oxide (ITO) [32,33]. The same effects were thought to be present in the molybdenum oxide deposition, to be able to control the stoichiometry as well as the conductivity of the deposited films.

Control over the properties and film stoichiometry was achieved either by using the Ar:$H_2$ atmosphere or by varying the deposition time and temperature. Thus, it was possible tailoring the reduced molybdenum oxide ($MoO_x$, $2 < x \leq 3$) thin film properties to an ideal design for any specific application. For instance, more transparent near-stoichiometric films can be useful in optoelectronic devices. Alternatively, reduced films or mixed molybdenum oxide phases can be

* Corresponding author at: Departament de Física Aplicada, Universitat de Barcelona, Barcelona, Spain.
*E-mail addresses:* nicolau97lopez@gmail.com (N. Lopez-Pinto), jbertomeu@ub.edu (J. Bertomeu).

https://doi.org/10.1016/j.apsusc.2021.150285
Received 31 July 2020; Received in revised form 19 May 2021; Accepted 31 May 2021
Available online 6 June 2021

preferred for application that demand better electrical transport. The conditions and sputtering atmosphere that may better adapt to each possible application are investigated in this work.

## 2. Experimental

### 2.1. Preparation of $MoO_3$ thin films

Two series of reduced molybdenum oxide samples (*SERIES* 1 and *SERIES* 2) were deposited by RF magnetron sputtering. The RF magnetron sputtering device was an AJA ATC Orion Series 8 HV confocal sputtering with three guns tilted 3° from the normal in a confocal geometry and a rotating substrate holder. The frequency signal used for turning on the plasma was 13.56 MHz. The sputtering device disposed of 3 mass flow controllers with 20 sccm of full scale. One was used to distribute Ar, the second one distributed $O_2$ and the third one supplied a forming gas mixture of 3.5% $H_2$ and 96.5% of Ar. A target of ceramic molybdenum oxide ($MoO_3$) with a purity of 99.995% and 3-inch diameter (~7.62 cm) × 6 mm thickness was used. A base pressure of $2.5 \times 10^{-6}$ Torr or lesser was achieved before every deposition.

Depositions were made onto an n-type c-Si ([1 0 0]) wafer and Corning 1737F glass. The thin oxide layer on the wafer had been removed by 60 s immersion in a 1% hydrofluoric (HF) acid solution. The glass substrates were cleaned with soap and 2-propanol, before being dried by blowing $N_2$ on top.

*SERIES* 1 consisted of three sets of 5 samples each. Each set was deposited in a different reactive atmosphere and varying chamber pressure (from 3 mTorr to 11 mTorr), as listed in Table 1.

No intentional heating of the substrates was applied, the power density at 3.3 W/cm$^2$ (150 W, 3″ target), 3 min of pre-sputtering before 12 min of deposition, gas flow fixed at full-scale for all atmospheres, oxygen and hydrogen partial flow being 3.5% (e.g. in a total of 20 sccm of gas flow there would be 19.3 sccm of Ar and 0.7 sccm of $O_2$ or $H_2$). Also, rotation of the sample holder was fixed at 10 rpm on its axis to ensure homogeneity in the film deposition, and target to substrate distance was set to 15 cm. These conditions remained constant for all the samples listed in Table 1.

*SERIES 2* consisted in two sets of samples deposited in an Ar:$H_2$ atmosphere at 3 mTorr with varying deposition times (from 1.5 to 12 min) in order to grow thinner films (see Table 2). The first set was deposited at room temperature (RT) (i.e. without intentional heating) while the second one was deposited at temperature set point of 100 °C. All other deposition conditions, such as gas flow or target to substrate distance, were the same as in *SERIES* 1, as well as for the cleaning procedures employed. Note that all the samples at 100 °C were thinner than their equivalent at RT.

**Table 1**
Listing of the samples deposited in SERIES 1 with the corresponding measured thickness in nanometers (nm) for every sample.

| Sample name | Reactive Atmosphere | Pressure (mTorr) | Thickness (nm) |
|---|---|---|---|
| A3 | Argon | 3 | 33.3 |
| A5 | | 5 | 35.9 |
| A7 | | 7 | 33.4 |
| A9 | | 9 | 30.1 |
| A11 | | 11 | 25.2 |
| AO3 | Argon + Oxygen | 3 | 33.7 |
| AO5 | | 5 | 24.3 |
| AO7 | | 7 | 18.7 |
| AO9 | | 9 | 14.1 |
| AO11 | | 11 | 12.9 |
| AH3 | Argon + Hydrogen | 3 | 28.9 |
| AH5 | | 5 | 32.9 |
| AH7 | | 7 | 28.1 |
| AH9 | | 9 | 26.3 |
| AH11 | | 11 | 23.5 |

**Table 2**
Listing of the samples deposited in SERIES 2 alongside the measured thickness of each sample in nanometers.

| Sample name | Deposition temperature (°C) | Time (min) | Thickness (nm) |
|---|---|---|---|
| S2-1 | RT | 1.5 | 7.3 |
| S2-3 | | 3 | 9.4 |
| S2-6 | | 6 | 16.5 |
| S2-12 | | 12 | 26.3 |
| S2T-1 | 100 | 1.5 | 6.6 |
| S2T-3 | | 3 | 8.8 |
| S2T-6 | | 6 | 14.4 |
| S2T-12 | | 12 | 23.5 |

### 2.2. Thickness determination: Ellipsometry

Sample thickness was studied by ellipsometry with a Plasmos SD2300 Ellipsometer at a wavelength of 632.8 nm with an incident angle of 60°. These measurements were done on the samples deposited on polished Si wafers.

### 2.3. Composition: XPS

X-ray photoelectron spectroscopy (XPS) analysis was carried out to get the composition of the samples. The device used was a PHI 5500 Multitechnique System (Physical Electronics®) with an Aluminum K-alpha X-ray source (1486.6 eV) which was calibrated with the $3d_{5/2}$ line of Ag, perpendicular to the analyzer axis. Stoichiometry was computed from the analysis of the O 1 s peaks and the Mo 3d peaks.

For the analysis of the peaks, a Shirley background type and Gaussian-Lorentzian overlapping curves were used. Molybdenum has a doublet peak due to the spin–orbit splitting with separation of ~3.2 eV between peaks [34], which was the only constraint we used when deconvoluting the curves. That is why different peak characteristics were obtained for each sample, but always keeping the required distance between doublet peaks.

### 2.4. Optical properties

Optical transmittance ($T_{meas}$) and reflectance ($R_{meas}$) spectra were measured with a PerkinElmer LAMBDA 950 spectrophotometer with a 150 mm integrating sphere, wavelengths varying from 300 nm (UV) to 1200 nm (near IR), which is the range that covers most of the Sun's AM1.5 spectrum. These measurements were done for the films deposited on the glass substrates.

The $T_{meas}$ and $R_{meas}$ spectra were used to find the absorption coefficient (α). Optical bandgap was computed by fitting the well-known "Tauc-plot", $(\alpha h\nu)^n = A\,(h\nu\text{-}E_g)$. From the relation between α and the energy of the incident photon, the bandgap energy $E_g$ of each sample could be found [35]. As indirect allowed transitions ($n = 1/2$) are often considered for nanocrystalline or amorphous films, this was also considered for the films studied here. The $MoO_3$ is reported to have an indirect band gap value between 2.7 and 3.5 eV [14,36–39].

To accurately determine the bandgap, linear regressions were evaluated at every point of the Tauc Plot, and the optical bandgap value was taken from the fitting where the linear regression coefficient ($\rho^2$) maximized, as further described in [40].

### 2.5. Electrical properties

Transfer length measurements (TLM) were realized with a Keithley 2601B source meter unit. The electrical contacts consisted of a stack of Au and Ag layers deposited by thermal evaporation on top of the $MoO_x$ samples both on Si wafers and glass substrates. Shadow masks defined the shape of the deposited contacts. Five different contact distances were used for the TLM measurement: $d$ = 1, 0.7, 0.5, 0.4 and 0.3-mm. The

contact width ($Z$) was 1.5 cm. Conductivity of the samples was afterwards computed by averaging the conductivity at each contact distance.

## 3. Results and discussion

### 3.1. Thickness and deposition rate

To understand the characteristics of the deposited samples, thickness -or its equivalent, deposition rate- is one of the foremost parameters to consider. Fig. 1 shows the evolution of the deposition rate versus pressure. While in the Ar and Ar:$H_2$ atmospheres the behavior was similar and the deposition rate did not differ much, the Ar:$O_2$ showed a different pattern, the higher deposition pressure the lower deposition rate. The "screening" of activated oxygen particles might be the cause of the decrease, this is, $O_2$ dissociates into $O^0$ particles ($O_2 + e^- \rightarrow 2O^0$) which are more chemically reactive and easily absorbed on surfaces, "poisoning" them. Those $O^0$ particles are to be absorbed into the target's surface and reduce the net surface of $MoO_3$ being bombarded by the plasma, thus screening the sputtering process.

In the Ar:$H_2$ atmosphere, the hydrogen was expected to associate with the sputtered particles to form bronzes once deposited ($H_xMo_x^{5+}Mo_{1-x}^{6+}O_3$). However, the bronzes are thermodynamically unstable and eventual removal of oxygen and hydrogen to form water should occur, leaving behind a more reduced state of molybdenum ($MoO_2$). Like this, an oxygen-deficient film grows with co-existing phases in it [30].

For the second set of series, it was aimed to improve the transmittance of the prior films by reducing their thickness while being able to maintain the other properties. It was also aimed to be able to control the sample stoichiometry even more by making depositions on a slightly hotter substrate (100 °C). For those purposes, deposition time was varied from 1.5 to 12 min and for each deposition time two samples were compared, one at RT and one at 100 °C.

The deposition rate was not constant; it evolved in a non-linear way. Thinner samples had a higher deposition rate than thicker ones, meaning that the growth rate of the film decreased after the initial layers of the film had been deposited. For this reason, the sample thickness was hard to predict. In the case of the series with temperature, the deposition rate of the films was generally slower than at RT. As the sample surface was at higher temperature, particles were less bounded and more propense to leave the surface, especially the lighter ones (i.e. oxygen). Accordingly, samples prepared at 100 °C manifested more metallic than the ones at RT, as will be shown after the XPS measurements shown below.

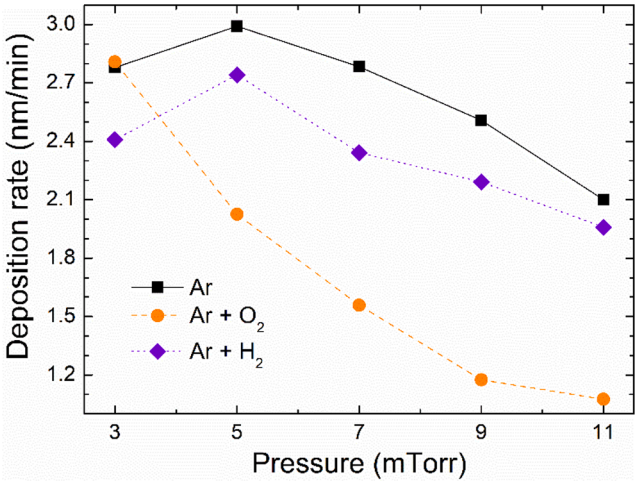


**Fig. 1.** Dependence of the deposition rate of samples in SERIES 1 with the deposition pressure in mTorr for each atmosphere. (Squares for Ar atmosphere, circles for Ar:$O_2$ and diamonds for Ar:$H_2$).

### 3.2. XPS analysis

The Mo3d core level spectra studied by XPS for some samples of *SERIES 1* are represented in Fig. 2, which shows the evolution of the different oxidation states over the increase of pressure. Along with the oxygen core-level spectra, the stoichiometry of the samples was computed. The deconvoluted blue curves in Fig. 2 show the $Mo^{6+}$ states while the green curves show the $Mo^{5+}$ states. For the $Mo^{6+}$ oxidation state, the obtained binding energy values of the lowest energy peak (the right one) were 232.7 ± 0.1 eV for all deconvolutions and the $Mo^{5+}$ oxidation state were 231.6 ± 0.5 eV. It should be noted that similar compositional results were obtained for the Ar atmosphere at 3 mTorr and the Ar:$H_2$ atmosphere at 11 mTorr. The ratio oxygen to molybdenum (O/Mo) was computed by dividing the total area of oxygen in the deconvolution by the total deconvoluted area of molybdenum, which leads to values between 2.74 and 2.98 as shown in Fig. 3. The samples prepared in the oxygen atmosphere were nearly stoichiometric, having higher O/Mo ratios than samples prepared in different atmospheres. In the case of Ar:$H_2$ atmosphere, the samples were less stoichiometric than in Ar and presented lower O/Mo ratios. The declining could be deduced looking at the XPS results in Fig. 2. The Ar:$H_2$ samples exhibit the $Mo^{5+}$ oxidation state independently of the deposition pressure, whereas the ones in the Ar atmosphere did not ($Mo^{5+}$ states disappear in samples above 7 mTorr). This is in agreement with the computed stoichiometry values (Fig. 3), which match the raw observations from the studied Mo3d core level spectra. The reduced oxidation states can be related to oxygen vacancies in the deposited films, indicating that the amount of oxygen missing in the film can be controlled either by the deposition pressure or the applied atmosphere.

The procedure of the XPS peak fitting used for the second series shown in Fig. 4 was the same as for *SERIES 1*, the primary condition we applied was a peak distance of ~3.2 eV between the doublet peaks. In this case, the binding energies associated with the lower energy peak were 232.9 ± 0.1, 232.0 ± 0.3 and 230.6 ± 0.4 eV for the $Mo^{6+}$, $Mo^{5+}$ and $Mo^{4+}$ respectively. The O/Mo ratio for these samples varied between 2.58 and 2.87, as presented in Fig. 5, where differences can be appreciated between 1.5 min samples and 12 min samples. The longer deposition time, the less stoichiometric grew the films. Samples prepared at 100 °C had oxygen deficiency either due to the presence of $Mo^{5+}$ states or the presence of $Mo^{4+}$ states, which would not contribute to generating oxygen vacancies. Note that by increasing the temperature of the substrate and the deposition chamber, it would be possible to control film stoichiometry in an Ar:$H_2$ atmosphere.

### 3.3. Optical properties

Regarding the optical properties of the films, the $T_{meas}$ and $R_{meas}$ were studied in the visible and near-infrared part of the spectrum to determine the average transmittance of the deposited film (weighted with the Sun's AM1.5 spectra irradiance using equation (1)) and the bandgap of the samples.

$$\langle T \rangle = \int_{300nm}^{1200nm} T(\lambda) E_{e,\lambda normalized}^{AM1.5}(\lambda) d\lambda \quad (1)$$

Fig. 6 shows the evolution of the average transmittance of the samples over the deposition pressure for each atmosphere in the inset. Thinner films were expected to be more transparent than the thicker ones, which was confirmed as the transmittance rises with the pressure in the same atmosphere. This result is further demonstrated by the samples prepared in *SERIES 2* (see Fig. 7), even though, it was not the only factor that affected the layer transmittance. The composition, in a less effective way, also affected the optical behavior of the films, the Ar:$H_2$ series were the less transparent while the Ar:$O_2$ ones were the more transparent (this could be fairly compared using samples of similar thickness which would be the Ar:$O_2$ at 5 mTorr and the Ar and Ar:$H_2$ at

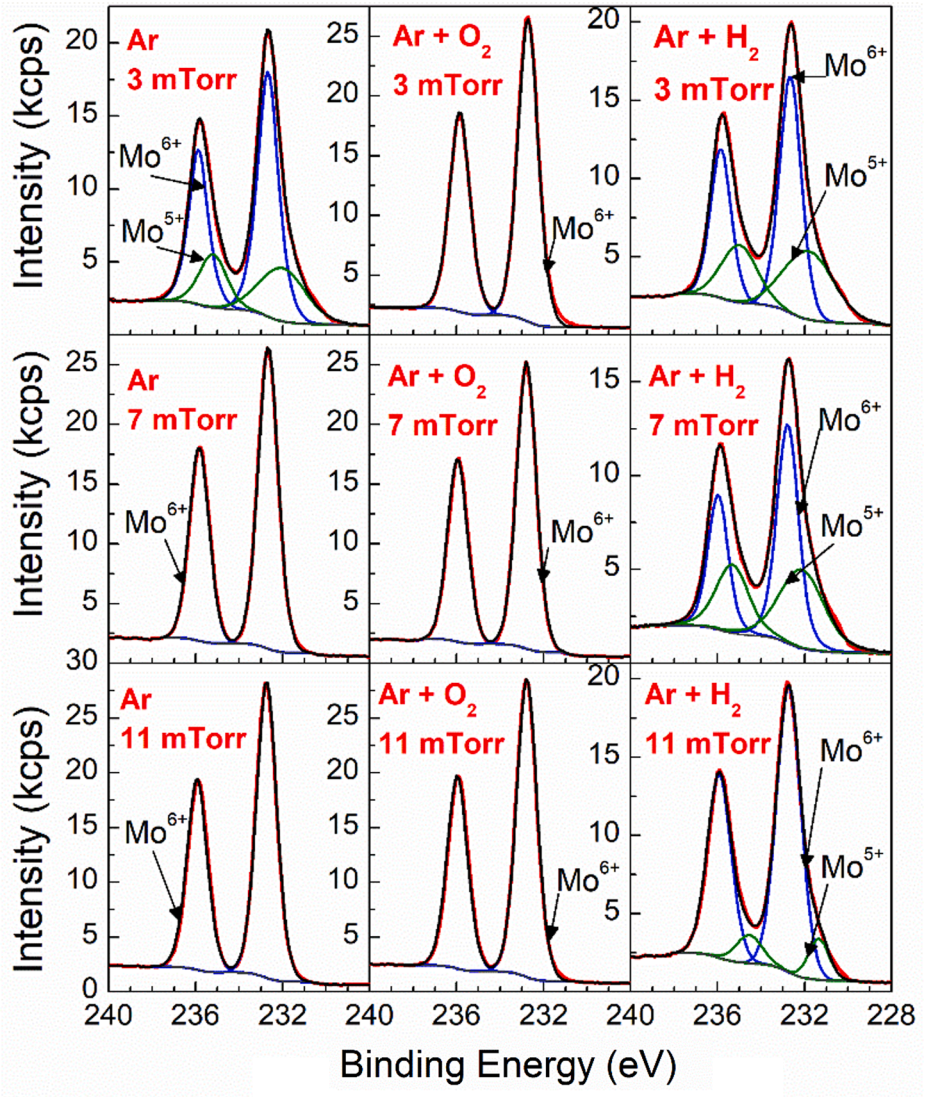


**Fig. 2.** XPS analyzed molybdenum core level spectra peaks of SERIES 1 for 3, 7, 11 mTorr samples in each atmosphere in the first, second and third row respectively. Blue lines are the deconvolution of the $Mo^{6+}$ peaks and green lines are for the $Mo^{5+}$ peaks. The intensity is displayed in counts per second (cps). The 3d peaks were centered in 232.7 eV and 232.6 eV for $Mo^{6+}$ and $Mo^{5+}$ respectively. (For interpretation of the references to color in this figure legend, the reader is referred to the web version of this article.)

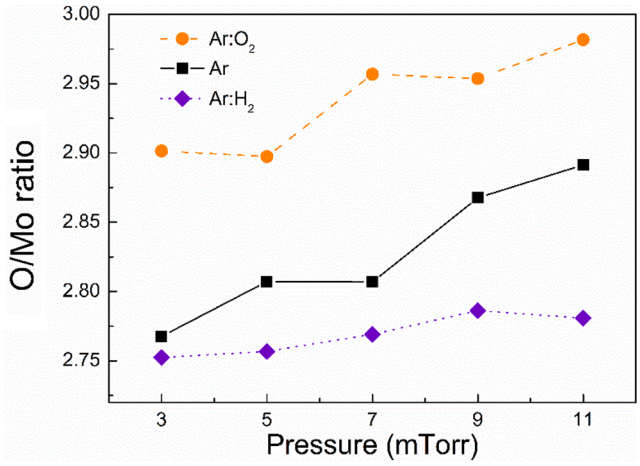


**Fig. 3.** Ox/Mo ratio for SERIES 1 computed from the XPS analysis for each deposition pressure. A clear distinction might be observed between each atmosphere, with increasing ratio values for increasing pressures.

11 mTorr, see Table 1). The oxidation states present in the film slightly influenced the optical transmittance as it could be appreciated in the case of the Ar and Ar:$H_2$ series. Despite the Ar samples being more transparent than the Ar:$H_2$ ones, they are thicker, and this is due to the latter ones presenting more oxygen vacancies. These oxygen vacancies are evidenced by a sub-bandgap absorption peak centred at ~850 nm [36] which is only present in the Ar and Ar:$H_2$ samples, not in the Ar:$O_2$ ones that are more stoichiometric (near to $MoO_3$), as it can be appreciated in Fig. 6 by a rise of the absorption coefficient around these wavelengths.

Optical bandgap calculations were done as explained in *2.4,* using $T_{meas}$ and $R_{meas}$ spectra to compute α (an example of this evaluation is depicted in Fig. 8). Evaluation of the band gap energy was made as proposed in [28] , which resulted in values between 2.83 and 3.5 eV with a relative error of less than 5% with no visible trend or relation amongst them. These values are in good agreement with the ones reported in the literature [14,36–39].

Referring to the desired transmittance improvement in *SERIES 2*, samples which deposition time was 1 min 30 s (the thinner ones) had around 90% average transmittance when weighted with the Sun's AM1.5 spectra. Samples prepared at 100 °C were moderately less transmitting despite the reduced states. In Fig. 7 it can be appreciated that there was almost no difference between samples prepared at RT and 100 °C, but that transmittance rapidly decreased with the thickness, a

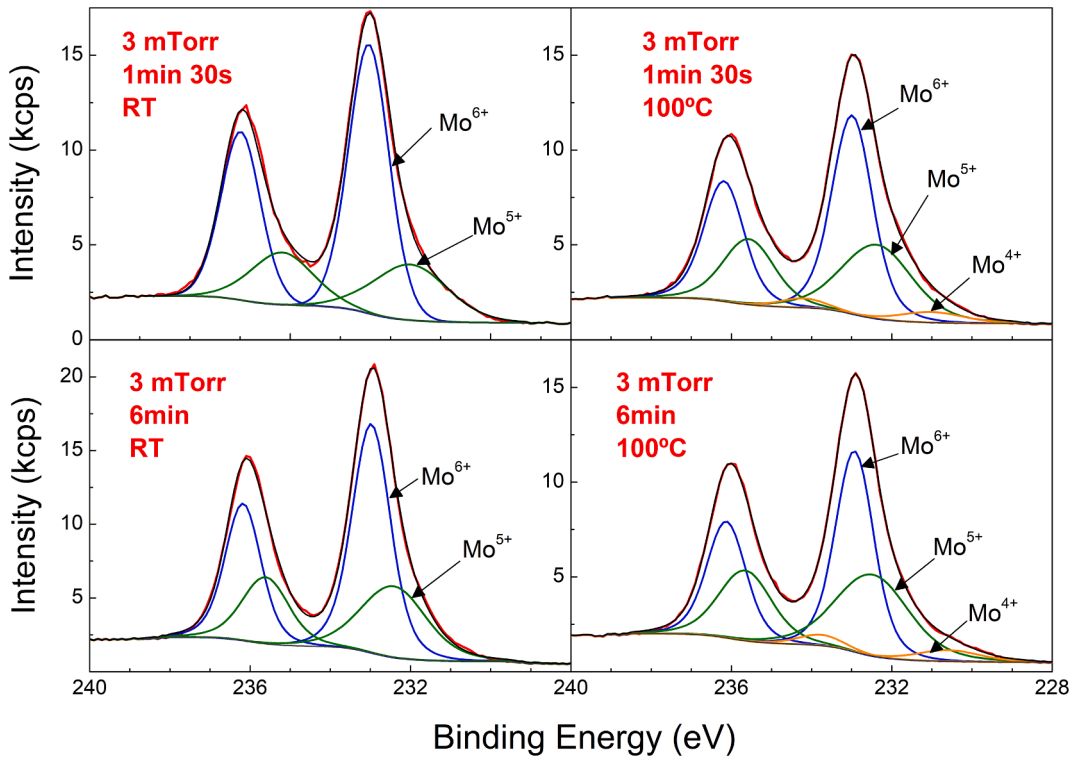


**Fig. 4.** XPS molybdenum peaks analyzed for the 1 min 30 s and 6 min samples in SERIES 2 (RT and 100 °C included). Blue lines correspond to $Mo^{6+}$ peaks, green lines to $Mo^{5+}$ deconvolved peaks and orange lines correspond to $Mo^{4+}$ deconvolutions. The positions of the 3d peaks were 232.9, 232.0 and 230.6 eV for the $Mo^{6+}$, $Mo^{5+}$ and $Mo^{4+}$ respectively. (For interpretation of the references to color in this figure legend, the reader is referred to the web version of this article.)

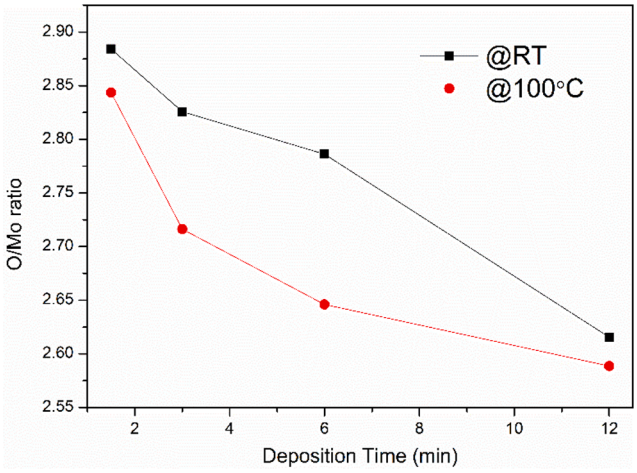


**Fig. 5.** Stoichiometry of the samples in SERIES 2 for every deposition time for the 100 °C samples and RT samples. There is an appreciable tendency of diminishing the O-Mo ratio, the more time invested in depositing in the Ar:$H_2$ atmosphere at RT and 100 °C.

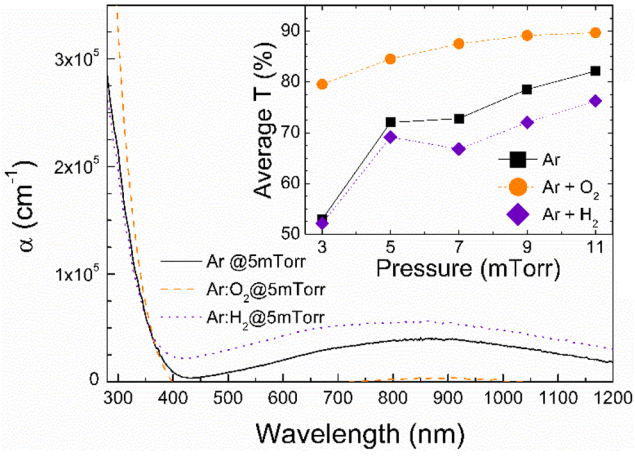


**Fig. 6.** The absorption coefficient of the 5mTorr samples in SERIES 1 for the visible spectra and near-infrared (300 nm to 1200 nm). Straight-line corresponds to the Ar atmosphere, dashed to Ar:$O_2$ and dotted to Ar:$H_2$. The inset shows the variation of the average transmittance of SERIES 1 for every pressure and atmosphere.

difference of less than 20 nm made a decrease on the transmittance of ~45%. Understanding on the influence of the film thickness and the composition to the transmittance of the film could be better achieved with this samples, thickness predominates over the composition, even though the latter has a slight influence on it, as it can be observed in Fig. 6 and Fig. 7.

On the evaluation of the optical bandgap energy, the same method as in *SERIES 1* was used. The computed values varied from 2.92 to 3.46 eV, which stayed within a similar range as the samples in *SERIES 1* and values reported in the literature. In Fig. 8 it can be observed a trend in the bandgap energy that gets narrower as the sample thickness increases. This phenomenon agrees with the XPS results, samples that get their stoichiometry reduced have more defects (e.g. oxygen vacancies, among other defects for the fact of the film being amorphous). They need less energy for the indirect allowed transitions to take place (additional band tail energy states are available between the valence and the conduction bands due to defects). The presence of those defects was also denoted by the Urbach energy [41], which increased from 200 meV for the thinner films to values higher than 1 eV for the thickest ones (1.25 eV the highest), a signal of a larger absorption front created by the defects as mentioned earlier.

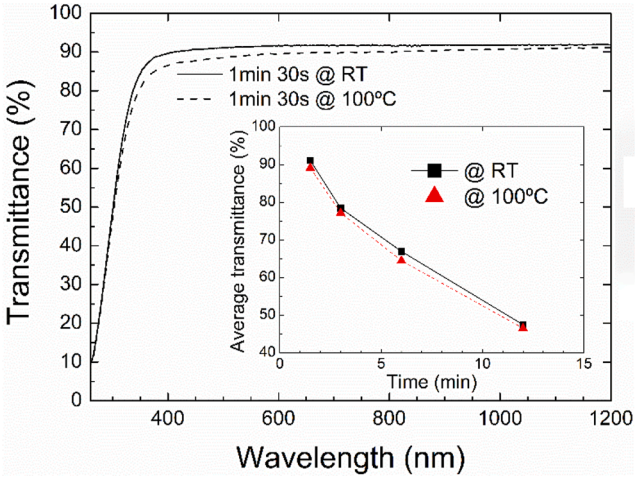


**Fig. 7.** Transmittance of the 1.5 min samples in SERIES 2 for the visible spectra and near-infrared (300–1200 nm). Straight-line corresponded to the RT samples and dashed to 100 °C samples. The inset shows the variation of the average transmittance of SERIES 2 for every deposition time and temperature.

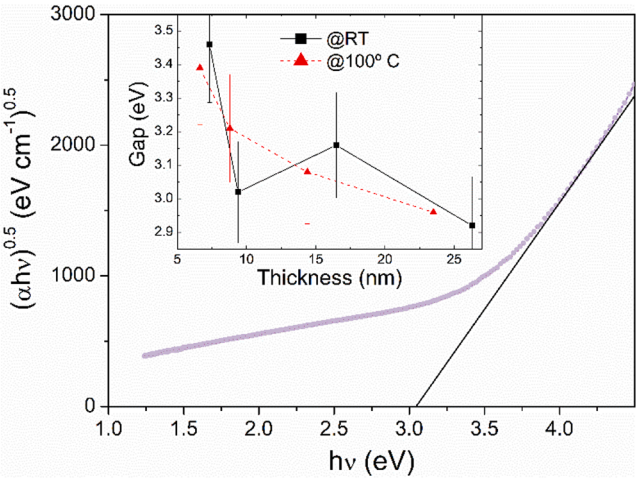


**Fig. 8.** Example of the Tauc plot used to determine the indirect optical bandgap value for all samples with the corresponding "best" regression computed with the method explained in 2.4. Additionally, an inset of the bandgap values versus the sample thickness for SERIES 2. The estimated error for the gap values is ~ 5%.

### 3.4. Electric characterization

The electric characterization of the films was performed through TLM, which consisted in measuring the resistance through the I-V curve for each contact distance. The following equation afterwards deduced the conductivity of the samples:

$$\sigma = \frac{1}{\rho} = \frac{d}{RZt} \tag{2}$$

being $t$ the sample thickness, $R$ the measured resistance at a given distance, $Z$ the width of the contacts and $d$ the distance between them.

As a general observation for each atmosphere, the samples grown at lower pressure presented a higher conductivity (see Fig. 9). This difference in the conductivity of the samples could be attributed to their composition. That is, samples deposited at lower pressure were more conductive as they had a more reduced stoichiometry (see Fig. 3). On the other hand, more stoichiometric samples had considerably lower conductivity. There are orders of magnitude difference between samples

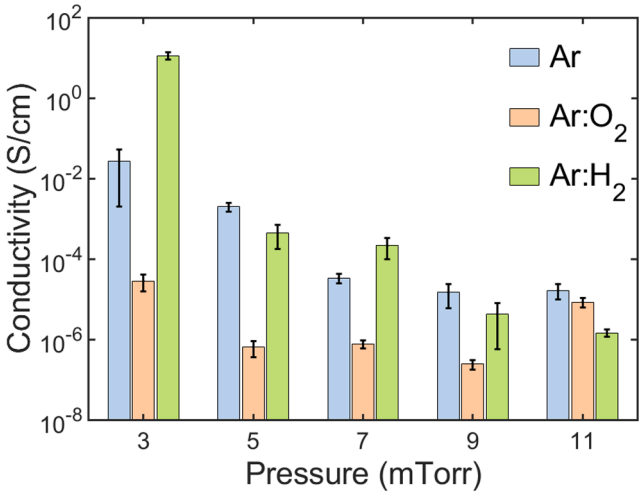


**Fig. 9.** Conductivity of the samples of *SERIES 1* in a logarithmic scale with their corresponding error bar. A diminishing of the conductivity can be observed as the pressure increases due to the reduction in the thickness and the films being more stoichiometric. For each pressure the conductivity of the Ar, Ar:$O_2$ and Ar:$H_2$ atmospheres are shown from left to right respectively.

prepared at 3 mTorr compared to the ones at 9 and 11 mTorr, both for Ar and Ar:$H_2$ atmospheres.

The optical and electric behavior of the films grown in the Ar:$H_2$ atmosphere can be explained mostly by their stoichiometry. They present a higher amount of $Mo^{5+}$ states (that denote a presence of oxygen vacancies) and, for instance, they are more metallic. This composition reduces the transmittance of the films as there is more absorption inside the film. Consequently, they present a lower transmittance as expected for a less stoichiometric metal oxide. The absence of oxygen is higher in the samples of *SERIES 2* and therefore their conductivity is higher. The transmittance is also higher in some of them, denoting the relevance of the thickness (which governs over the composition as already stated) in this characteristic of the film.

The conductivity of samples in *SERIES 2* was measured the same way as for *SERIES 1*. A notable difference was appreciated (about 1 order of magnitude or more, see Fig. 10) for samples deposited at 100 °C

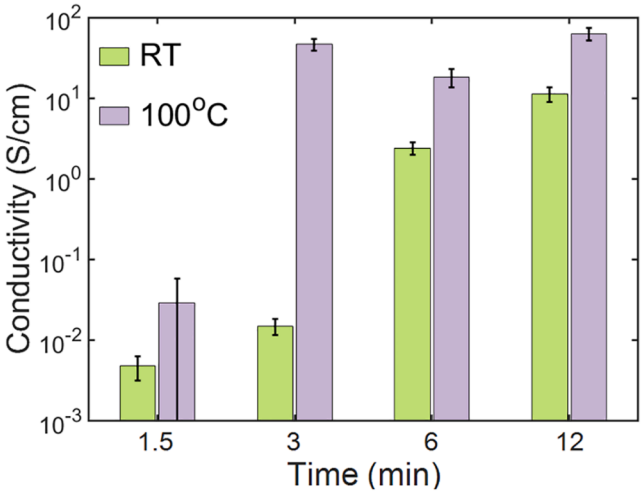


**Fig. 10.** Conductivity of the samples of SERIES 2 in a logarithmic scale with their corresponding error bar. For each deposition time the conductivity for samples prepared at RT is displayed in the left and the ones at high temperature in the right. A clear increase was observed when increasing the thickness. An anomalous result can be observed for 3mTorr at high temperature with unknown origin.

compared to those at RT, in agreement with the reduced oxidation states present in the higher temperature samples. Again, thicker samples were the most conductive due to their composition being reduced. An anomaly was observed for the sample at 3 min with unknown cause.

### 3.5. Final insights

By depositing *SERIES 1,* a better understanding of the influence of the Ar:$H_2$ atmosphere was accomplished. Even though samples prepared in the Ar:$H_2$ atmosphere had lower transmittance due to the absence of some oxygen in the films, their behavior was almost the same as in the Ar atmosphere. Especially when the deposition pressure increased, thus supporting the idea that hydrogen in the atmosphere may react with the film and the sputtered particles to form bronzes [30]. The resulting film are reduced as it is observed in Fig. 3, leading to changes in the conductivity.

Improvements in the modulation of the film characteristics, such as higher conductivity (at 3 mTorr) or stoichiometry control (significant difference at 3 and 5mTorr especially) through the Ar:$H_2$ atmosphere arouse interest in a more-in-depth study of this deposition conditions. Therefore, a second series were deposited at 3 mTorr pressure with substantial differences in the resulting film characteristics.

The deposition of *SERIES 2* helped in the understanding of the reduction in the film. Bronzes that leave the film expected from the results of [30] seemed to have its effect enhanced by temperature, and for instance, $Mo^{4+}$ states appeared. As the deposition rate was slightly slower when depositing at 100 °C, the oxygen-hydrogen association could be favored when the sputtered particles were reaching the substrate. Supporting this hypothesis was the fact that in the XPS analysis, $Mo^{4+}$ states could be observed, which were related to the presence of $MoO_2$ metastable configurations in the layer. At RT, this effect was negligible, and only oxygen vacancies were observed.

This phenomenon did not influence the transmittance of the films as seen in Fig. 7 but affected the deposition rate and the conductivity of the samples. As they were more metallic due to the presence of the $Mo^{4+}$ states, they, consequently, were more conducting. Transmittance was mostly affected by the film thickness, while the conductivity was predominantly conditioned by the composition of the deposited film. A great drop in the average transmittance was observed through the samples from *SERIES 2*, but the conductivity increased in a rather smooth behavior.

Variations in the film characteristics arise out of deposition temperature changes, which could let us deposit a reduced molybdenum film with the specific characteristic we desire once fully understood its behavior for each application the film is designed. For instance, if the desired device were a gas sensor, the deposition conditions would be sputtering in the Ar:$H_2$ atmosphere with low pressure and temperature and for 20 min or even more to ensure good conductivity and a relatively high thickness. On the other hand, if the desired device were a solar cell, the deposition conditions would be sputtering in an Ar:$H_2$ atmosphere with low pressure and room temperature (unless the vacancies in the film were not enough at RT) during 3–4 min in order to have a highly transparent film with oxygen vacancies to act as a selective HTL contact and relatively good conductivity.

## 4. Conclusions

Reduced molybdenum thin films were deposited in different atmospheres (*SERIES 1)* and at different temperatures *(SERIES 2)*. Films prepared in the Ar:$H_2$ atmosphere presented oxygen vacancies at every deposition pressure and temperature, resulting more conductive than in other atmospheres. Overall, some benefits could be appreciated in *SERIES 1* by sputtering in the Ar:$H_2$ atmosphere, such as a possibility to reduce the stoichiometry of the film and improvements in the conductivity. Nevertheless, changes in the sputtering atmosphere alone were not enough to control every aspect of the deposited film (e.g. there was a small difference in transmittance when depositing in Ar atmosphere vs Ar:$H_2$ atmosphere). The films prepared afterwards at higher temperatures exhibited $Mo^{4+}$ states and therefore were more conductive. Transmittance, which was highly influenced by film thickness, reached values around 90% in the thinner films.

As oxygen to molybdenum ratios varied between 2.74 and 2.98 for the first series and from 2.58 to 2.87 in the second series, control over the deposited film stoichiometry can be achieved in an Ar:$H_2$ atmosphere by appropriately tuning either the deposition time or the chamber pressure. Furthermore, control over film parameters that depend on the stoichiometry may be also tuned by varying the temperature. Some devices that could only be developed in a laboratory environment could be brought to the industry plane by sputtering with the Ar:$H_2$ atmosphere as one of their processes.

## Credit authorship contribution statement

**Nicolau Lopez-Pinto:** Conceptualization, Methodology, Formal analysis, Software, Writing - review & editing, Data curation, Investigation. **Thomas Tom:** Conceptualization, Data curation, Investigation. **Joan Bertomeu:** Methodology, Writing - review & editing, Supervision, Funding acquisition, Resources, Validation. **Jose Miguel Asensi:** Data curation, Writing - review & editing, Investigation, Software, Validation, Formal analysis. **Eloi Ros:** Investigation, Resources. **Pablo Ortega:** Supervision, Funding acquisition. **Cristobal Voz:** Data curation, Writing - review & editing, Supervision, Resources, Funding acquisition, Validation, Resources.

## Declaration of Competing Interest

The authors declare that they have no known competing financial interests or personal relationships that could have appeared to influence the work reported in this paper.

## Acknowledgement

This research has been supported by the Spanish Ministerio de Economía, Industria y Competitividad (ENE2016-78933-C4-1-R and ENE2016-78933-C4-2-R), Ministerio de Ciencia e Innovación (PID2019-109215RB-C4-1 and PID2019-109215RB-C4-3) and the European Regional Development Fund. One of the authors (T. Tom) acknowledges the support of the Secretaria d'Universitats i Recerca de la Generalitat de Catalunya and European Social Fund (2019 FI_B 00456).

## References

[1] H. Hosono, Recent progress in transparent oxide semiconductors: Materials and device application, Thin Solid Films. 515 (2007) 6000–6014, https://doi.org/10.1016/j.tsf.2006.12.125.
[2] P.S. Patil, R.S. Patil, Studies on spray pyrolyzed molybdenum trioxide thin films, Bull. Mater. Sci. 18 (1995) 911–916, https://doi.org/10.1007/BF02745283.
[3] J. Geissbühler, J. Werner, S. Martin De Nicolas, L. Barraud, A. Hessler-Wyser, M. Despeisse, S. Nicolay, A. Tomasi, B. Niesen, S. De Wolf, C. Ballif, 22.5% efficient silicon heterojunction solar cell with molybdenum oxide hole collector, Appl. Phys. Lett. 107 (2015), https://doi.org/10.1063/1.4928747.
[4] J. Dréon, Q. Jeangros, J. Cattin, J. Haschke, L. Antognini, C. Ballif, M. Boccard, 23.5%-efficient silicon heterojunction silicon solar cell using molybdenum oxide As hole-selective contact, Nano Energy. 70 (2020), https://doi.org/10.1016/j.nanoen.2020.104495.
[5] C. Battaglia, X. Yin, M. Zheng, I.D. Sharp, T. Chen, S. McDonnell, A. Azcatl, C. Carraro, B. Ma, R. Maboudian, R.M. Wallace, A. Javey, Hole selective MoOx contact for silicon solar cells, Nano Lett. 14 (2014) 967–971, https://doi.org/10.1021/nl404389u.
[6] J. Bullock, Y. Wan, Z. Xu, S. Essig, M. Hettick, H. Wang, W. Ji, M. Boccard, A. Cuevas, C. Ballif, A. Javey, Stable dopant-free asymmetric heterocontact silicon solar cells with efficiencies above 20%, ACS Energy Lett. 3 (2018) 508–513, https://doi.org/10.1021/acsenergylett.7b01279.
[7] L.G. Gerling, S. Mahato, A. Morales-Vilches, G. Masmitja, P. Ortega, C. Voz, R. Alcubilla, J. Puigdollers, Transition metal oxides as hole-selective contacts in silicon heterojunctions solar cells, Sol. Energy Mater. Sol. Cells. 145 (2016) 109–115, https://doi.org/10.1016/j.solmat.2015.08.028.

[8] X.Y. Jiang, Z.L. Zhang, J. Cao, W.Q. Zhu, High stability and low driving voltage green organic light emitting diode with molybdenum oxide as buffer layer, Solid. State. Electron. 52 (2008) 952–956, https://doi.org/10.1016/j.sse.2008.01.017.
[9] N. Oka, H. Watanabe, Y. Sato, H. Yamaguchi, N. Ito, H. Tsuji, Y. Shigesato, Study on MoO3−x films deposited by reactive sputtering for organic light-emitting diodes, J. Vac. Sci. Technol. A Vacuum, Surfaces, Film. 28 (2010) 886–889, https://doi.org/10.1116/1.3328822.
[10] C.V. Ramana, V.V. Atuchin, H. Groult, C.M. Julien, Electrochemical properties of sputter-deposited MoO 3 films in lithium microbatteries, J. Vac. Sci. Technol. A Vacuum, Surfaces, Film. 30 (2012) 04D105, https://doi.org/10.1116/1.3701763.
[11] R. Yordanov, S. Boyadjiev, V. Georgieva, L. Vergov, Characterization of thin MoO3 films formed by RF and DC-magnetron reactive sputtering for gas sensor applications, J. Phys. Conf. Ser. 514 (2014), https://doi.org/10.1088/1742-6596/514/1/012040.
[12] S.I. Boiadjiev, M. Markova, M. Rasovska, R.S. Iordanov, RF reactive sputtering of MoO3 thin films for sensor applications, Proceedings of Electronics' 2005, Vol 5, pp. 141–145. ISBN: 954 438 521 5.
[13] D. Mutschall, K. Holzner, E. Obermeier, Sputtered molybdenum oxide thin films for NH3 detection, Sens. Actuators, B Chem. 36 (1996) 320–324, https://doi.org/10.1016/S0925-4005(97)80089-5.
[14] K. Inzani, M. Nematollahi, F. Vullum-Bruer, T. Grande, T.W. Reenaas, S. M. Selbach, Electronic properties of reduced molybdenum oxides, Phys. Chem. Chem. Phys. 19 (2017) 9232–9245, https://doi.org/10.1039/c7cp00644f.
[15] S. Subbarayudu, V. Madhavi, S. Uthanna, Growth of MoO3 films by RF magnetron sputtering: studies on the structural, optical, and electrochromic properties, ISRN Condens. Matter Phys. 2013 (2013) 1–9, https://doi.org/10.1155/2013/806374.
[16] G. Cebisli, S. Asubay, Y.S. Ocak, Reactively sputtered MoO3 thin films and temperature dependence of electrical properties of an Ag/MoO3/n-Si Diode, J. Ovonic Res. 14 (2018) 405–414.
[17] S.H. Mohamed, O. Kappertz, J.M. Ngaruiya, T.P. Leervad Pedersen, R. Drese, M. Wuttig, Correlation between structure, stress and optical properties in direct current sputtered molybdenum oxide films, Thin Solid Films. 429 (2003) 135–143, https://doi.org/10.1016/S0040-6090(03)00068-3.
[18] F. Jankowski, L.R. Schrawyer, Reactive sputtering of molybdenum, Thin Solid Films. 194 (1990) 61–71.
[19] D. Manno, A. Serra, M. Di Giulio, G. Micocci, A. Tepore, Physical and structural characterization of tungsten oxide thin films for NO gas detection, Thin Solid Films. 324 (1998) 44–51, https://doi.org/10.1016/S0040-6090(97)01205-4.
[20] M. Sook Oh, B. Seob Yang, J. Ho Lee, S. Ha Oh, U. Soo Lee, Y. Jang Kim, H. Joon Kim, M. Soo Huh, Improvement of electrical and optical properties of molybdenum oxide thin films by ultralow pressure sputtering method, J. Vac. Sci. Technol. A Vacuum, Surfaces, Film. 30 (2012), 031501, https://doi.org/10.1116/1.3692753.
[21] X. Fan, G. Fang, P. Qin, N. Sun, N. Liu, Q. Zheng, F. Cheng, L. Yuan, X. Zhao, Deposition temperature effect of RF magnetron sputtered molybdenum oxide films on the power conversion efficiency of bulk-heterojunction solar cells, J. Phys. D. Appl. Phys. 44 (2011), https://doi.org/10.1088/0022-3727/44/4/045101.
[22] I.H. Yoo, Y.J. Lee, S.S. Kalanur, H. Seo, Assembly of nonstoichiometric molybdenum oxide on Si as p-n junction photocathode for enhanced hydrogen evolution, Appl. Catal. B Environ. 264 (2020), 118542, https://doi.org/10.1016/j.apcatb.2019.118542.
[23] C.V. Ramana, V.V. Atuchin, L.D. Pokrovsky, U. Becker, C.M. Julien, Structure and chemical properties of molybdenum oxide thin films, J. Vac. Sci. Technol. A Vacuum, Surfaces, Film. 25 (2007) 1166–1171, https://doi.org/10.1116/1.2747628.
[24] C.V. Ramana, V.V. Atuchin, V.G. Kesler, V.A. Kochubey, L.D. Pokrovsky, V. Shutthanandan, U. Becker, R.C. Ewing, Growth and surface characterization of sputter-deposited molybdenum oxide thin films, Appl. Surf. Sci. 253 (2007) 5368–5374, https://doi.org/10.1016/j.apsusc.2006.12.012.
[25] M. Ferroni, V. Guidi, G. Martinelli, P. Nelli, M. Sacerdoti, G. Sberveglieri, Characterization of a molybdenum oxide sputtered thin film as a gas sensor, Thin Solid Films. 307 (1997) 148–151, https://doi.org/10.1016/S0040-6090(97)00279-4.
[26] S. Catalán, L. Álvarez-Fraga, E. Salas, R. Ramírez-Jiménez, A. Rodriguez-Palomo, A. De Andrés, C. Prieto, Charge mobility increase in indium-molybdenum oxide thin films by hydrogen doping, Appl. Surf. Sci. 386 (2016) 427–433, https://doi.org/10.1016/j.apsusc.2016.05.109.
[27] M. Kozejova, V. Latyshev, V. Kavecansky, H. You, S. Vorobiov, A. Kovalcikova, V. Komanicky, Evaluation of hydrogen evolution reaction activity of molybdenum nitride thin films on their nitrogen content, Electrochim. Acta. 315 (2019) 9–16, https://doi.org/10.1016/j.electacta.2019.05.097.
[28] Y. Wang, Q. Huang, C. Wei, D. Zhang, Y. Zhao, X. Zhang, Improvement of electrical and optical properties of molybdenum doped zinc oxide films by introducing hydrogen, Appl. Surf. Sci. 258 (2012) 8797–8801, https://doi.org/10.1016/j.apsusc.2012.05.093.
[29] M. Greenblatt, Molybdenum Oxide Bronzes with Quasi-Low-Dimensional Properties, Chem. Rev. 88 (1988) 31–53, https://doi.org/10.1021/cr00083a002.
[30] A. Borgschulte, O. Sambalova, R. Delmelle, S. Jenatsch, R. Hany, F. Nüesch, Hydrogen reduction of molybdenum oxide at room temperature, Sci. Rep. 7 (2017) 1–9, https://doi.org/10.1038/srep40761.
[31] T.H. Fleisch, G.J. Mains, An XPS study of the UV reduction and photochromism of MoO3 and WO3, J. Chem. Phys. 76 (1982) 780–786, https://doi.org/10.1063/1.443047.
[32] K. Zhang, F. Zhu, C.H.A. Huan, A.T.S. Wee, Effect of hydrogen partial pressure on optoelectronic properties of indium tin oxide thin films deposited by radio frequency magnetron sputtering method, J. Appl. Phys. 86 (1999) 974–980, https://doi.org/10.1063/1.370834.
[33] C.S. Moon, J.G. Han, Low temperature synthesis of ITO thin film on polymer in Ar/H2 plasma by pulsed DC magnetron sputtering, Thin Solid Films. 516 (2008) 6560–6564, https://doi.org/10.1016/j.tsf.2007.11.028.
[34] XPS Interpretation of Molybdenum, (n.d.). https://xpssimplified.com/elements/molybdenum.php (accessed July 9, 2020).
[35] J. Tauc, Optical properties and electronic structure of amorphous Ge and Si, Mater. Res. Bull. 3 (1968) 37–46, https://doi.org/10.1016/0025-5408(68)90023-8.
[36] J. Werner, J. Geissbühler, A. Dabirian, S. Nicolay, M. Morales-Masis, S. De Wolf, B. Niesen, C. Ballif, Parasitic absorption reduction in metal oxide-based transparent electrodes: application in perovskite solar cells, ACS Appl. Mater. Interfaces. 8 (2016) 17260–17267, https://doi.org/10.1021/acsami.6b04425.
[37] S.S. Sunu, E. Prabhu, V. Jayaraman, K.I. Gnanasekar, T.K. Seshagiri, T. Gnanasekaran, Electrical conductivity and gas sensing properties of MoO3, Sens. Actuators, B Chem. 101 (2004) 161–174, https://doi.org/10.1016/j.snb.2004.02.048.
[38] H. Simchi, B.E. McCandless, T. Meng, J.H. Boyle, W.N. Shafarman, Characterization of reactively sputtered molybdenum oxide films for solar cell application, J. Appl. Phys. 114 (2013), https://doi.org/10.1063/1.4812587.
[39] A.L. Fernandes Cauduro, Z.E. Fabrim, M. Ahmadpour, P.F.P. Fichtner, S. Hassing, H.G. Rubahn, M. Madsen, Tuning the optoelectronic properties of amorphous MoOx films by reactive sputtering, Appl. Phys. Lett. 106 (2015), https://doi.org/10.1063/1.4921367.
[40] B.D. Viezbicke, S. Patel, B.E. Davis, D.P. Birnie, Evaluation of the Tauc method for optical absorption edge determination: ZnO thin films as a model system, Phys. Status Solidi Basic Res. 252 (2015) 1700–1710, https://doi.org/10.1002/pssb.201552007.
[41] T. He, J. Yao, Photochromism of molybdenum oxide, J. Photochem. Photobiol. C Photochem. Rev. 4 (2003) 125–143, https://doi.org/10.1016/S1389-5567(03)00025-X.